Deep–Sea Research I 156 (2020) 103190

Contents lists available at ScienceDirect

Deep-Sea Research Part I

journal homepage: http://www.elsevier.com/locate/dsri

Enhanced but highly variable bioturbation around seamounts in the northwest Pacific

Zifei Yang, Qiankun Qian, Min Chen *, Run Zhang, Weifeng Yang, Minfang Zheng, Yusheng Qiu

College of Ocean and Earth Sciences, Xiamen University, Xiamen, 361102, China

ARTICLE INFO

Keywords:
Sedimentation
Bioturbation
^{230}Th
^{210}Pb
Seamounts
Northwest Pacific

ABSTRACT

Seamounts are a unique ecosystem in marine environment, but the relevant understanding is limited. In this study, sedimentation and bioturbation around the Pako Guyot of Magellan, and the Lamont, Scripps, Arnold, and Pot Guyots of Marcus-Wake seamounts in the northwest Pacific were evaluated using $^{230}Th_{ex}$ and $^{210}Pb_{ex}$ as tracers. Our results showed that the linear sedimentation rate and the mass accumulation rate ranged from 0.12 to 2.50 mm/ka and from 0.06 to 1.14 kg/m^2/ka with averages of 1.27 ± 0.80 mm/ka and 0.49 ± 0.30 kg/m^2/ka respectively. The accumulation flux of organic carbon in surface sediments was estimated to be 0.10–4.52 g C/m^2/ka. The bioturbation coefficients ranged from 1.01 to 27.1 cm^2/a with an average of 10.8 ± 9.2 cm^2/a, which is higher than those in abyssal sediments or predicted by traditional empirical equations. The enhanced bioturbation supports the view that seamounts are hotspots for pelagic and benthic organisms. The bioturbation intensity showed a great variability with the maximum around 40 km away from the edge of seamount summit. The bioturbation coefficient correlated positively with sedimentation rate and accumulation flux of organic carbon in surface sediments, indicating that the supply of organic matter is a main driving force for enhanced bioturbation around the seamounts. The increase in sedimentary organic matter promotes the activities of benthic organisms. More research is needed to gain a deep understanding of bioturbation in seamounts in the context of future climate change.

1. Introduction

Bioturbation, sediment transport processes including reworking and borrowing through benthic organisms (especially macrobenthos), leads to significant changes in community structure and early diagenesis, and further affects biogeochemical cycling in sediments (Kristensen et al., 2012). In deep-sea environments, bioturbation dominates the transport of surface sediments (Tromp et al., 1995). Almost all particles that settle down to the seabed are disturbed several times before being buried deeply (Wheatcroft, 1992). Bioturbation alters physical and chemical properties of sediments by mixing new sediments with old ones (Meadows et al., 2012). Destruction of chemical gradients in porewater increases the supply of oxygen and food, thus accelerates diffusion-limiting reactions such as dissolution of minerals (opal, calcite and apatite, etc.), and increases mineralization rate of organic matter (Arndt et al., 2013; Chakrabarty and Das, 2007; Henderson et al., 1999; Lohrer et al., 2004). Naturally, bioturbation disturbs origin signals recorded in sediments and biases understanding of paleoenvironmental change (Charbit et al., 2002; Henderson et al., 1999; Hutson, 1980; Leuschner et al., 2002).

A variety of models have been developed to quantify bioturbation intensity, including random walks model, transition-matrix model, lattice-automaton model and stochastic differential model (Boudreau, 1986; Boudreau et al., 2001; Shull, 2001; Wheatcroft et al., 1990). Bio-diffusion model, especially one-dimensional steady-state eddy diffusion model, has been widely applied in studies of sediment bioturbation (Guinasso and Schink, 1975; Meysman et al., 2003; Smith et al., 1993, 1997; Suckow et al., 2001). In this model, bioturbation and sedimentation are considered to be similar to diffusion and advection respectively. Bioturbation coefficient (D_B) and mixed depth (L) are used to describe bioturbation intensity mathematically (Boudreau, 1994, 1998; Middelburg et al., 1997; Teal et al., 2008). The D_B value represents the movement rate of particles, which is in proportional to particle diffusion. The L value denotes the depth where particles are frequently mixed. Both D_B and L can be estimated based on tracer profile in a sediment core. ^{234}Th ($T_{1/2}$ = 24.1 d) and ^{210}Pb ($T_{1/2}$ = 22.23 a) are radioisotopes used widely to quantify biotubation (Boudreau, 1994; Lecroart et al., 2010; Teal et al., 2008). ^{210}Pb is suitable for long-term

* Corresponding author.
E-mail address: mchen@xmu.edu.cn (M. Chen).

https://doi.org/10.1016/j.dsr.2019.103190
Received 9 August 2019; Received in revised form 25 November 2019; Accepted 4 December 2019
Available online 7 December 2019

bioturbation in deep-sea sediments, while ^{234}Th is more suitable for high-frequency conditions in coastal environments (Boudreau, 1986; Reed et al., 2006; Smith et al., 1993). Although many studies have been conducted on D_B or L in sediments, most of them focused on nearshore or north Atlantic. Little is known about bioturbation in the northwest Pacific. Globally, bioturbation intensity has been found to correlate positively with sedimentation rate and organic matter accumulation flux, and correlate negatively with water depth (Boudreau, 1994; Middelburg et al., 1997; Tromp et al., 1995). It remains unclear whether these relationships remain true in the northwest Pacific, where many seamounts exist and sedimentation rate is only a few millimeters per millennium.

Seamounts are ubiquitous intermediate-scale (0–10 km) topographic features on the seabed (Wessel et al., 2010). Based on global bathymetric data at 30 arc-sec resolution, 33,452 seamounts (above 1000 m) and 138,412 knolls (200–1000 m height) are identified, who cover approximately 21% of ocean's floor (Yesson et al., 2011). However, only a few hundred seamounts have been surveyed until now. How seamounts affect environmental complexity, biological patchiness, biogeochemical cycle and sedimentary processes are not fully understood (Turnewitsch et al., 2013). Many studies have focused on biodiversity and biomes in the seamounts, as they act as hotspots for biological activities. However, not all of seamounts receive enough nutrients from overlying waters, the high benthic biomass in seamounts remains to be explained (McClain, 2010; Wilson et al., 1987). Bioturbation is an indicator of benthos diversity and activity, but studies on bioturbation in seamounts are rare (Levin and Thomas, 1989; Yang et al., 2011). Levin and Thomas (1989) found that infaunal activities in the seamount cap were more active than in the perimeter of summit in the central Pacific due to its slow current, but no significant relationship was observed between bioturbation coefficient (0.6–3.0 cm^2/a) and current velocity. In addition, a positive relationship between bioturbation coefficient (1.59–8.64 cm^2/a) and organic carbon content was observed around the seamounts of the northwest Pacific (Yang et al., 2011).

Seamounts are a unique ecosystem in oceanic environments and are hotspots for pelagic and benthic organisms. However, knowledge of sedimentation, bioturbation, and carbon fluxes around seamounts remains scarce, in part, due to the remoteness, limited sampling, and the need in multidisciplinary approach. In this study, bioturbation intensity at several Guyots in the northwest Pacific was evaluated by $^{210}Pb_{ex}$ tracer using a bio-diffusion model. In order to clarify the factors affecting the D_B around the seamounts, sedimentation rate was determined by $^{230}Th_{ex}$ tracer. The role of sedimentary process and deposition flux of particulate organic matter in regulating bioturbation around the seamounts was discussed. The spatial variability of bioturbation intensity around the seamounts was depicted to understand the effect of topographic changes. Our objective is to test the hypothesis that seamounts provide unique topographic environment for accumulation of particulate organic matter in sediments, especially at the foot of seamounts, which stimulates bioturbation activity of benthic organisms.

2. Material and methods

2.1. Study areas

Many seamount clusters are located on the northwest Pacific plate. Here, a total of 12 sediment cores were collected from the Magellan Seamounts Cluster and the Marcus-Wake Seamounts Cluster between the northwest Pacific and the east Mariana Basin. Among them, seven sediment cores (MABC18, MAMC07, MABC06, MABC16, MAMC06, MABC02 and MABC11) were collected from the Pako Guyot centered at 15.7° N, 155.2° E, a large northeastern seamount belonging to the Magellan Cluster. The other five sediment cores (NAMC02, C1-MC1601, C1-MC1602, C3-MC1603 and C3-MC1604) were collected from Marcus-Wake Seamounts Cluster (Fig. 1).

The Pako Guyot is covered by cobalt-rich crusts. The summit is covered by foraminiferal ooze, with a minimum water depth of 1350 m and a slope between 0.5° and 2.0°. The edge of the summit is at depth of 1500–1650 m while the surrounding abyssal plain is about 5500 m depth. The average slope gradient from the summit to 4000 m depth is 10.9° (Wang et al., 2016; Zhu et al., 2011). Microgeomorphic units, like trench, ridge and depression, are well developed on the slope (Zhu et al., 2011). The bottom current around the Pako Guyot is affected by tides with seasonal variability, which is anticyclonic with the highest velocity at the summit and the lowest at the base. Besides, a northward current steadily presents in the eastern base of the mountain (Wang et al., 2016).

Several seamounts, including the Lamont, Scripps, Arnold, and Pot Guyots, locate around our sampling sites of the Marcus-Wake Seamount Cluster. The topography is more complicated than in the Pako Guyot. The heights of these seamounts range from 3656 m to 4022 m, and the base depth is about 5500 m. The Lamont Guyot is located at 21°30′ N, 160°00′ E with a height of 3656 m and a summit area of 1570 km^2. The uphill slope is 15.7° while that of downhill is 1.7° on average. The Scripps Guyot is located at 23°40′ N, 159°20′ E, with a height of 4022 m and a slope gradient of 1.7°. The Arnold Guyot is located at 21°10′ N, 158°15′ E with a summit area of 424 km^2 at the height of 3839 m. This Guyot rises 2.3° on the lower flanks and 11.3° on the upper flanks. The Pot Guyot lies at 19°30′ N, 160°10′ E, with a height of 3839 m and a slope of 10.8° (Smoot, 1989).

2.2. Sampling

Seven sediment cores were collected around the Pako Guyot by a multiple corer with an inner diameter of 9.5 cm during July–September 2012 onboard the *HAIYANG LIUHAO*. The other five cores were collected around the Marcus-wake seamounts by a multiple corer during a voyage in 2016 on board the *XIANGYANGHONG SHIHAO* (Table 1). The multiple corer used in our sampling is able to collect sediments without disturbance. All the cores were sampled below the carbonate compensation depth at a depth of about 4500 m (Berger et al., 1976), and consisted of deep sea red clay. After collection, the sediment core was sectioned at 1 cm intervals as soon as possible. The subsample was sealed in a clean polyethylene bag and stored frozen at -18 °C. In the land laboratory, sediment samples were freeze-dried for further analysis.

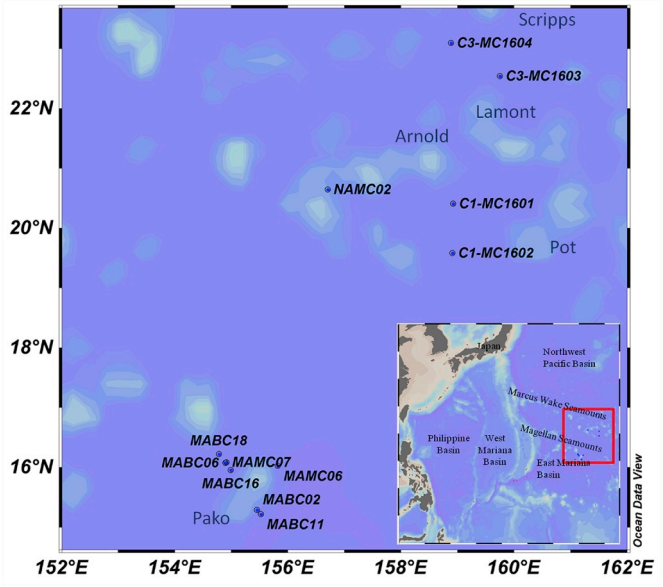

Fig. 1. Sampling locations around the seamounts in the northwest Pacific. Stations MABC18, MAMC07, MABC06, MABC16, MAMC06, MABC02 and MABC11 are located around the Pako Guyot of the Magellan seamount cluster, and stations NAMC02, C1-MC1602, C1-MC1601, C3-MC1603 and C3-MC1604 are located around the Pot, Lamont and Arnold seamounts of the Marcus-Wake seamount cluster.

Table 1
Samping location, water depth, porosity at the sediment-water interface (Φ_0), organic carbon content (C_{org}), organic carbon accumulation flux (F_{orgC}), linear sedimentation without compaction (s*), mass accumulation rate (r), and bioturbation coefficient (D_B) at each station.

Station	Longitude	Latitude	depth	Φ_0	C_{org}	F_{orgC}	s*	r	D_B
	(°E)	(°N)	(m)	(%)	(%)	(gC/m^2/ka)	(mm/ka)	(kg/m^2/ka)	(cm^2/a)
MABC18	154.787	16.222	5778	0.838	0.24	0.75 ± 0.08	0.75 ± 0.08	0.31 ± 0.03	2.03 ± 0.2
MAMC07	154.916	16.084	5445	0.777	0.25	0.66 ± 0.04	0.56 ± 0.03	0.26 ± 0.01	4.23 ± 0.65
MABC06	154.897	16.075	5497	0.848	0.40	4.52 ± 0.22	2.50 ± 0.14	1.14 ± 0.06	27.1 ± 4.5
MABC16	154.994	15.954	4629	0.806	0.18	0.10 ± 0.02	0.12 ± 0.02	0.06 ± 0.01	1.79 ± 0.25
MAMC06	155.825	16.025	5920	0.839	0.30	1.78 ± 0.09	1.87 ± 0.10	0.60 ± 0.03	22.4 ± 2.3
MABC02	155.459	15.288	5269	0.819	0.20	1.07 ± 0.09	1.12 ± 0.10	0.54 ± 0.05	9.9 ± 1.7
MABC11	155.529	15.216	5840	0.809	0.24	0.65 ± 0.05	0.63 ± 0.05	0.28 ± 0.02	3.21 ± 0.42
NAMC02	156.710	20.642	4570	0.767	0.19	0.58 ± 0.05	0.54 ± 0.05	0.30 ± 0.03	1.01 ± 0.13
C1-MC1601	158.924	20.406	5560	0.747	0.30	2.50 ± 0.12	2.35 ± 0.11	0.84 ± 0.04	19.98 ± 1.62
C1-MC1602	158.910	19.580	5645	0.806	0.29	1.58 ± 0.06	2.06 ± 0.09	0.54 ± 0.02	9.63 ± 0.91
C3-MC1603	159.754	22.540	5231	0.794	0.24	0.81 ± 0.05	1.06 ± 0.07	0.34 ± 0.02	8.16 ± 1.90
C3-MC1604	158.887	23.093	5520	0.729	0.26	1.72 ± 0.10	1.70 ± 0.11	0.67 ± 0.04	19.78 ± 2.39

2.3. Density and porosity

Sediment samples were weighted before and after freeze-dried to calculate dry density and porosity. Dry density is calculated by the following equation:

$$\rho_D = \frac{w_D}{\pi \times \left(\frac{D}{2}\right)^2 \times H - \frac{w_W - w_D}{\rho_{SW}}} \quad (1)$$

where ρ_D is dry density of sediments (g/cm^3), w_D and w_W are dry weight and wet weight respectively (g), D is the diameter of sediment core (9.5 cm), H is the height of subsample (1 cm in this study), and ρ_{SW} is density of seawater (1.025 g/cm^3).

The porosity is calculated as follows:

$$\varnothing = \frac{V_W}{V_T} = \frac{\frac{w_W - w_D}{\rho_{SW}}}{\frac{w_W - w_D}{\rho_{SW}} + \frac{w_D}{\rho_D}} \quad (2)$$

where Φ is porosity used to calibrate compaction effect in the sediment core.

2.4. ^{210}Pb, ^{226}Ra and ^{230}Th analysis

2.4.1. ^{210}Pb

The radioactivity of ^{210}Pb was determined by its 46.5 keV γ ray with a branch ratio of 4.25% via a high-purity germanium (HPGe) detector (GX3020, CANBERRA). The detection efficiency was calibrated using sediment standards DYhd2013-0544 and DYhd2013-0545 from National Institute of Metrology, China. The specific activity of ^{210}Pb was calculated by the following equation:

$$A = \sum_{i=1}^{n} \left(\frac{N_i}{t} - \frac{N_{b_i}}{t_b}\right) \times \frac{1}{\varepsilon_i Y_i m} \quad (3)$$

where A is specific activity of ^{210}Pb (Bq/kg), N_i and N_{b_i} are peak areas at 46.5 keV of the sample and the blank respectively, t and t_b are counting times for sample and blank respectively, ε_i is detection efficiency of ^{210}Pb (0.13 in this study), Y is branch ratio (4.25%), and m is the weight of sample (kg).

2.4.2. ^{226}Ra

The post-homogenized sediments were sealed in a polyethylene box at least 20 days until radioactive equilibrium between ^{222}Rn and ^{226}Ra was established. The radioactivity of ^{226}Ra was determined by γ spectrometry with a high-purity germanium (HPGe) detector (GX3020, CANBERRA) through its decay products ^{214}Pb and ^{214}Bi. The energy transitions are 295.2 keV (18.4%) and 351.9 keV (35.6%) of ^{214}Pb, and 609.3 keV (45.49%) and 1120.3 keV (14.91%) of ^{214}Bi. In previous studies, different γ ray lines were used to determine ^{226}Ra activity, such as 351.9 keV, 609.3 keV and 1120.3 keV γ rays (Yang et al., 2011); 295.2 keV and 609.3 keV γ rays (Suckow et al., 2001); 295.2 keV, 351.9 keV and 609.3 keV γ rays (Yang et al., 1986). In this study, peak areas at 295.2 keV, 351.9 keV, 609.3 keV and 1120.3 keV were determined simultaneously for samples collected from stations MABC06, MABC16, MABC18 and MAMC07. Our results showed that the specific activities of ^{226}Ra calculated from peak areas under the 295.2 keV were consistent with those under 609.3 keV, but the activities via the 351.9 keV and 1120.3 keV were inconsistent. The specific activity of ^{226}Ra from 351.9 keV γ ray was overestimated due to interference of ^{211}Bi, who emits a γ ray at 351.1 keV (12.91%) (Gilmore, 2008). The specific activity of ^{226}Ra from 1120.3 keV γ ray fluctuated greatly due to its low branch ratio (14.91%). Thus, only the peak areas under 295.2 keV and 609.3 keV were used to calculate specific activity of ^{226}Ra in this study. The detection efficiency of ^{226}Ra was calibrated using sediment standards DYhd2013-0544 and DYhd2013-0545 from National Institute of Metrology, China.

2.4.3. ^{230}Th

The specific activity of ^{230}Th was determined using the 67.7 keV γ ray with a branch ratio of 0.377%. In order to assess detection efficiency of ^{230}Th, ^{230}Th activity in sediment samples from cores MABC06 and MABC18 was determined by α and γ spectrometry simultaneously. After assuming that ^{230}Th activity obtained by α spectrometry is accurate, detection efficiency (ε) of γ spectrometry was calculated as follows:

$$\varepsilon = \frac{N}{A_\alpha Y m t} \quad (4)$$

where N is peak areas of the 67.7 keV γ ray, Y is the branch ratio (0.377%), t is the counting time (s), m is the mass of sediments (kg), and A_α is specific activity of ^{230}Th determined by α spectrometry (Bq/kg).

The determination of ^{234}U and ^{230}Th by α spectrometry follows a widely used method with ^{229}Th and ^{236}U as yield tracers (Chen et al., 2003; Yang et al., 2013; Zhang et al., 2004). In brief, 2–3 g of the pre-dried and homogenized sediments was first digested with $HClO_4$, HNO_3 and HF. The solution passed though a chloride-form anion resin column to separate Th from U. The eluents containing U and Th were electro-deposited on a stainless plate. The activity of ^{236}U, ^{234}U, ^{230}Th and ^{229}Th with energies of 4.493 MeV, 4.776 MeV, 4.687 MeV and 4.845 MeV was determained by α spectrometry (Qctête® Plus, ORTEC, USA) respectively.

Our results showed that the efficiency of ^{230}Th (67.7 keV) detected by the γ spectrometry based on equation (4) ranged from 0.1318 to 0.2198 with an average of 0.163 ± 0.020. The activity of ^{230}Th measured by γ spectrometry was calculated by the detection efficiency at a similar geometry.

The sedimentation rate was assessed based on excess activity of ^{230}Th (^{230}Th$_{ex}$), which is equal to the specific activity of ^{230}Th minus

that of ^{234}U. Since specific activity of ^{234}U in deep sea sediments is 1–2 orders of magnitude lower than ^{230}Th and varies a little vertically (Yang et al., 1986), the averaged specific activity of ^{234}U (23 Bq/kg) in the MABC06 and MABC18 sediments obtained by α spectrometry was used to calculate the $^{230}Th_{ex}$ in other samples. The resulting uncertainty of $^{230}Th_{ex}$ was much less than the counting error of ^{230}Th activity.

2.5. Organic carbon content

0.2–0.5 g of the dried sediments was transferred to a pre-combusted (450 °C, 4 h) permeable crucible and treated with 1 mol/L HCl for 4–6 h at 50 °C to remove inorganic carbon. After cooling, the sample was washed with Milli-Q water to pH = 7 and dried at 60 °C for 48 h 10 mg of the pre-treated sediments was wrapped into a tin capsule and analyzed using an elemental analyzer (Carlo Erba NC 2500) connected to a Thermo DELTA V isotopic ratio mass spectrometer. The detection limit and precision of carbon content were 0.1 μmol and better than 0.2%, respectively.

3. Results

3.1. Sedimentation rate derived from excess ^{230}Th

3.1.1. Profile of porosity and ^{230}Th

Although there are some fluctuations, the porosity generally decreases exponentially with increasing depth, showing the effect of sediment compaction (Fig. 2). The relationship between porosity and depth is used to calibrate compaction effect in calculation of linear sedimentation rate.

As shown in Fig. 3, the specific activity of ^{230}Th generally decreases with increasing depth at all stations due to radioactive decay. However, ^{230}Th is relatively constant in a few centimeters below the sediment-water interface, reflecting the mixing in the upper sediments. The ^{230}Th data in the mixed layer should be excluded when calculating sedimentation rate below.

3.1.2. Linear sedimentation rate

The compaction effect will reduce the thickness of lower deposits, thus underestimate the apparent linear sedimentation rate. In this study, the compaction effect is corrected based on the profile of porosity (Matsumoto and Wong, 1977). Briefly, the porosity Φ at depth x (cm) in a homogeneous sediment core is described as following equation:

$$\varnothing = (\varnothing_0 - \varnothing_\infty)e^{-\alpha x} + \varnothing_\infty \quad (5)$$

where Φ_0 and Φ_∞ represent porosity at sediment-water interface ($x = 0$) and fully compaction effect ($x = \infty$), respectively, α is a coefficient. By fitting the porosity to the depth in a sediment core, Φ_0, Φ_∞ and α is assessed.

The depth without compaction, x^* (cm), is calculated as follows:

$$x^* = \frac{1-\varnothing_\infty}{1-\varnothing_0}x + \frac{\varnothing_0-\varnothing_\infty}{\alpha(1-\varnothing_0)}e^{-\alpha x} - \frac{\varnothing_0-\varnothing_\infty}{\alpha(1-\varnothing_0)} \quad (6)$$

Assuming that deposition flux of $^{230}Th_{ex}$ (^{230}Th unsupported by its parent ^{234}U) to the seafloor is constant, and the mixing effect on $^{230}Th_{ex}$ is ignored, specific activity of $^{230}Th_{ex}$, A_i (Bq/kg) at a corrected depth x_i^* in the sediment core should be:

$$A_i = A_0 \exp\left(-\frac{\lambda_{Th}}{s^*}x_i^*\right) \quad (7)$$

where A_0 is the specific activity of $^{230}Th_{ex}$ at sediment-water interface (Bq/kg), λ_{Th} is decay constant of ^{230}Th (9.195×10^{-3} ka^{-1}), s^* is the linear sedimentation rate after correction for compaction (mm/ka).

Based on the relationship between specific activity of $^{230}Th_{ex}$ and x^* in our sediment cores, the linear sedimentation rates are calculated to be in a range of 0.12–2.50 mm/ka with an average of 1.27 ± 0.80 mm/ka (Table 1 and Fig. 4). For comparison, the sedimentation rate was estimated to be 0.10–2.15 mm/ka with an average of 0.89 ± 0.57 mm/ka without considering the compaction effect.

The sedimentation rates around seamounts in the northwest Pacific are consistent with those reported in the north Pacific, with a range of 0.4–4 mm/ka and an average of 1.70 ± 0.96 mm/ka (Druffel et al., 1984; Williams et al., 1978).

3.1.3. Mass accumulation rate

The mass accumulation rate (r) is not affected by compaction effect, which is calculated by the following equation:

$$A_i = A_0 \exp\left(-\frac{\lambda_{Th}}{r}m_i\right) \quad (8)$$

where A_i is the specific activity of $^{230}Th_{ex}$ (Bq/kg) at the average mass depth m_i of i-th section (kg/m^2). The mass depth $m(i)$ (kg/m^2) at layer i conforms to the following equation (Sanchez-Cabeza and Ruiz-Fernández, 2012):

$$m(i) = \sum_{j=1}^{j=i}\frac{\Delta m_i}{S} \quad (9)$$

where Δm_i is dry mass of section i (kg), S is cross-section of sediment core (m^2), and m_i is calculated as follows:

$$m_i = \frac{m(i-1)+m(i)}{2} \quad (10)$$

Based on the relationship between specific activity of $^{230}Th_{ex}$ and the m_i in a sediment core, the mass accumulation rate is calculated to be in a range of 0.06–1.14 kg/m^2/ka with an average of 0.48 ± 0.29 kg/m^2/ka (Fig. 5). For comparison, the mass accumulation rate of dust in our study areas was reported to range from 0.25 to 1 kg/m^2/ka (Rea, 1994; Windom, 1975). It seems that eolian deposition is a main source of abyssal sediments in the north Pacific.

Theoretically, the mass accumulation rate (r_c) can be calculated from s^* according to the following equation:

$$r_c = s^* \times \rho_D \times (1-\varnothing_0) \quad (11)$$

where r_c is the theoretically calculated mass accumulation rate (kg/m^2/ka), and ρ_D is dry density of sediment (kg/m^3). Our results showed a good positive linear correlation between r and r_c with a slope close to 1 ($r_c = 0.96 \cdot r + 0.01$, $r^2 = 0.999$, $p < 0.0001$), indicating that r and s^* are matched in this study.

3.2. Accumulation of organic matter

3.2.1. Organic carbon

The content of organic carbon (C_{org}) in surface sediments ranges from 0.18% to 0.40% with an average of 0.26 ± 0.06% (Table 1), which is close to the central North Pacific (0.21%–0.40%) (Müller and Suess, 1979), but slightly lower than the central equatorial Pacific (0.26%–0.68%) (Smith et al., 1996) and the northeast tropical Pacific (0.39%–0.48%) (Yang and Zhou, 2004). The highest content of organic carbon appeared at station MABC06 on the northern foot of Pako Guyot (0.40%), while the lowest (0.18%, station MABC16) on the northern slope. No significant difference in organic carbon content is observed in surface sediments from the Magellan and the Marcus-Wake seamounts. The low organic carbon content in surface sediments is consistent with low productivity in the subtropical Paicific.

3.2.2. Accumulation flux of organic carbon

The accumulation flux of organic carbon (F_{orgC}, gC/m^2/ka) is calculated as follows:

$$F_{orgC} = r \times C_{org} \times 10 \quad (12)$$

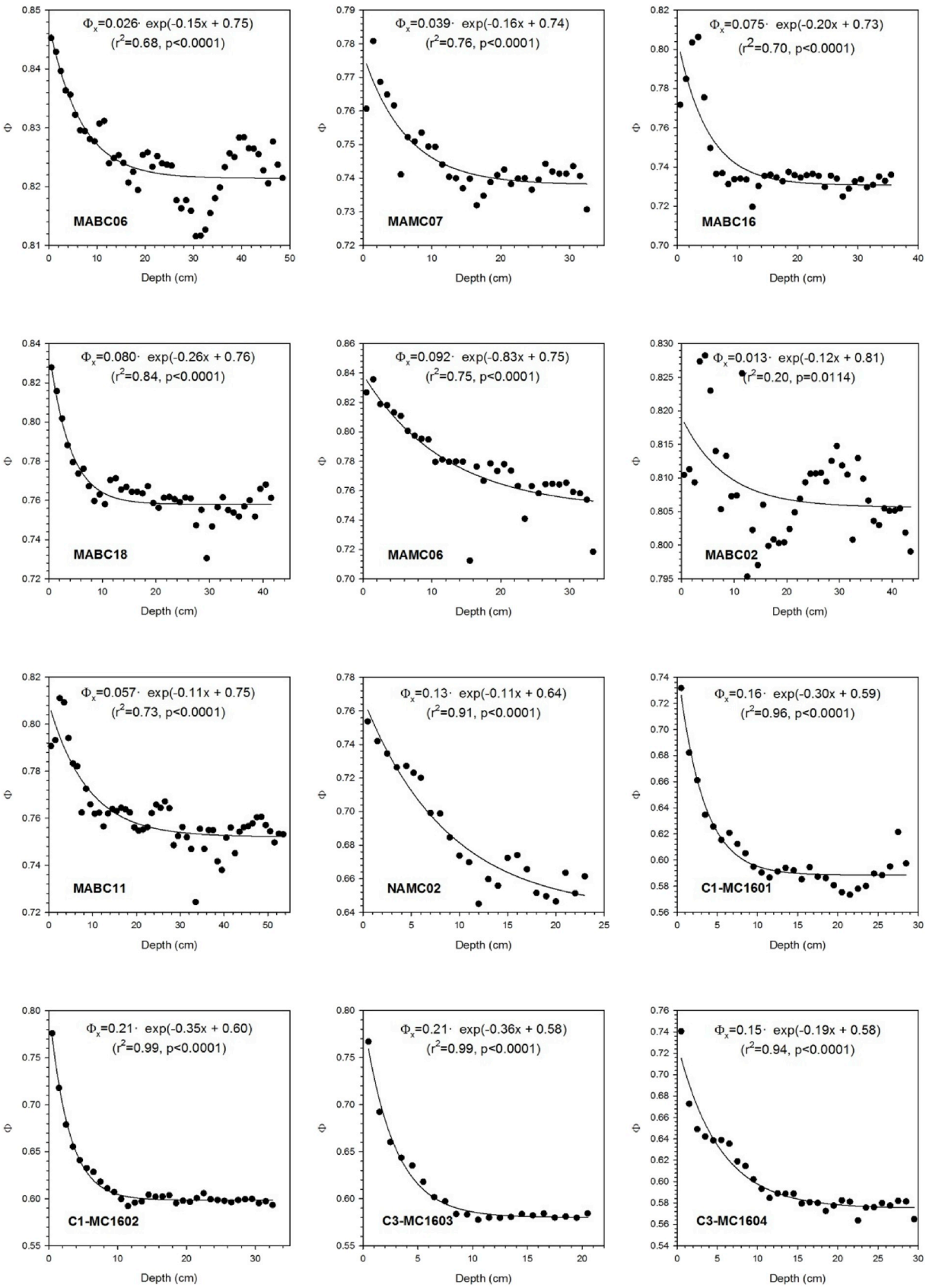

Fig. 2. Profiles of porosity in sediment cores. The x-axis is depth (cm), and the y-axis is porosity. The porosity shows an exponential decrease with depth. The fitting curve and equation is shown in each panel.

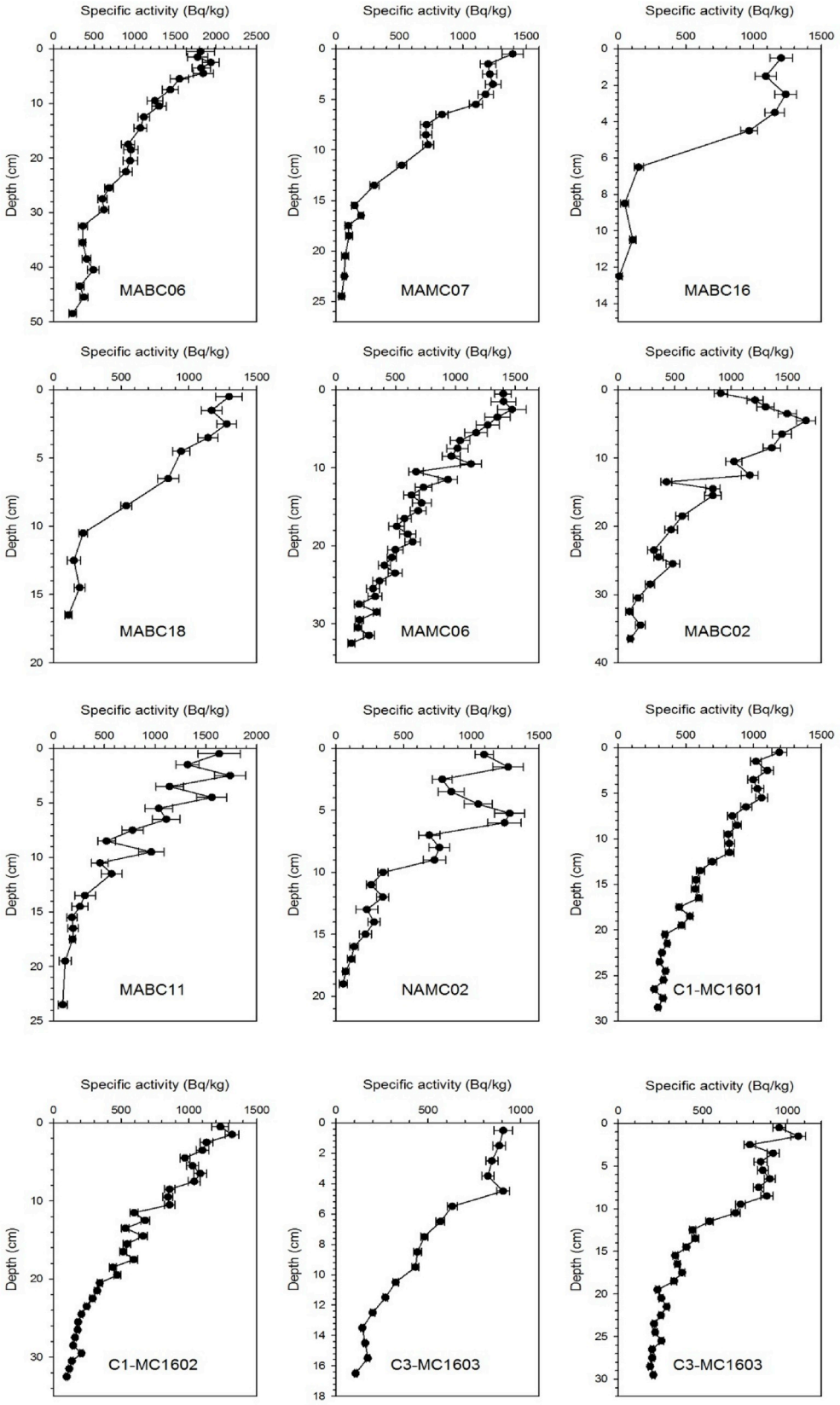

Fig. 3. Profiles of ^{230}Th in sediment cores. The x-axis is specific activity of ^{230}Th (Bq/kg) and the y-axis is depth (cm). Note that ^{230}Th activity is homogeneous in the upper 2–6 cm. ^{230}Th activity decreases exponentially with the depth below the mixed layer due to radioactive decay.

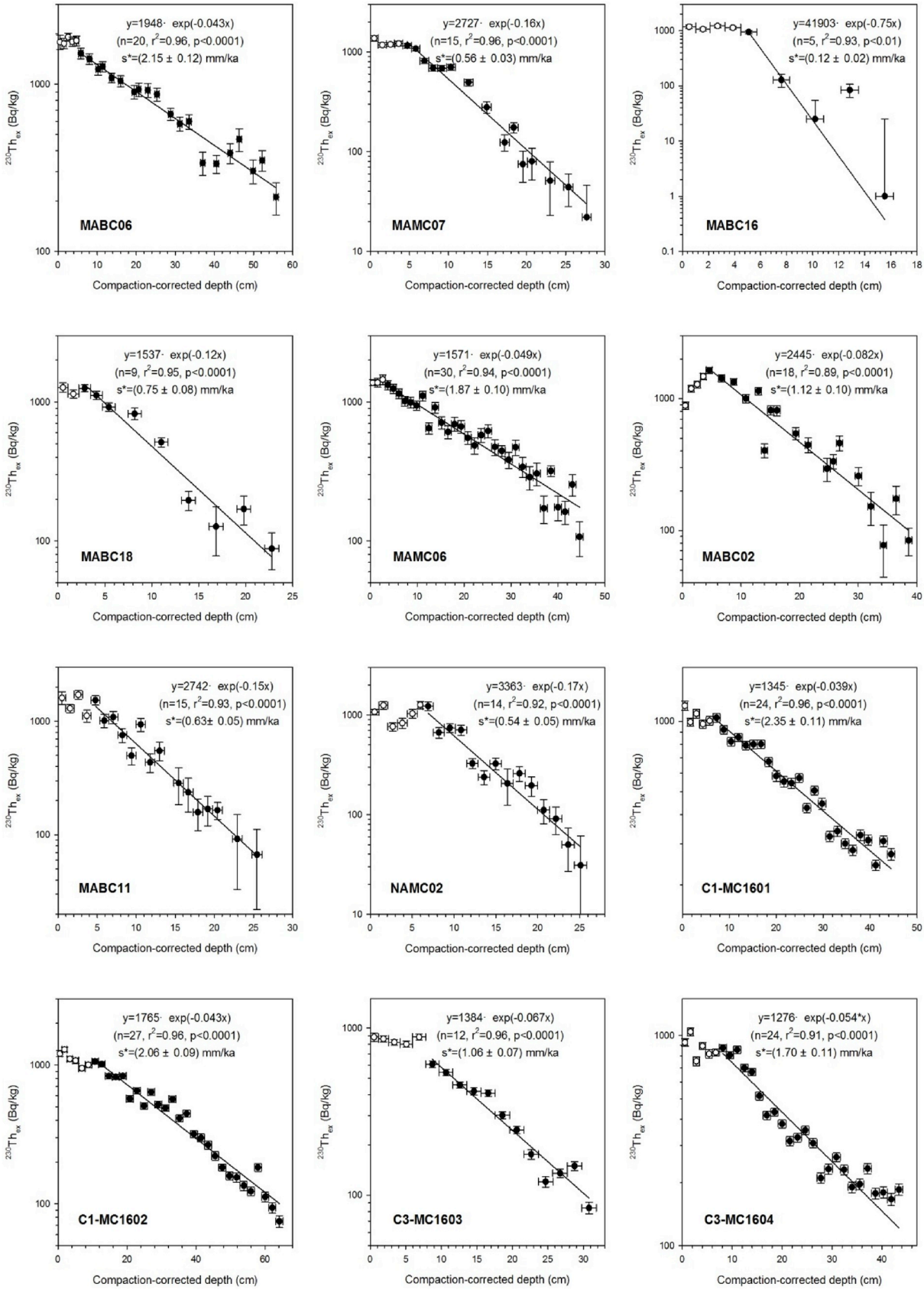

Fig. 4. The relationship between specific activity of $^{230}Th_{ex}$ (Bq/kg) and compaction-corrected depth (cm) in sediment cores. The fitting curve and equation are shown. Note that data in the mixed layer are shown in open circles, which is excluded in calculation of sedimentation rate. The estimated linear sedimentation rates are 2.15, 0.56, 0.12, 0.75, 1.87, 1.12, 0.63, 0.54, 2.35, 2.06, 1.06 and 1.70 mm/ka at stations MABC06, MAMC07, MABC16, MABC18, MAMC06, MABC02, MABC11, NAMC02, C1-MC1601, C1-MC1602, C3-MC1603 and C3-MC1604, respectively.

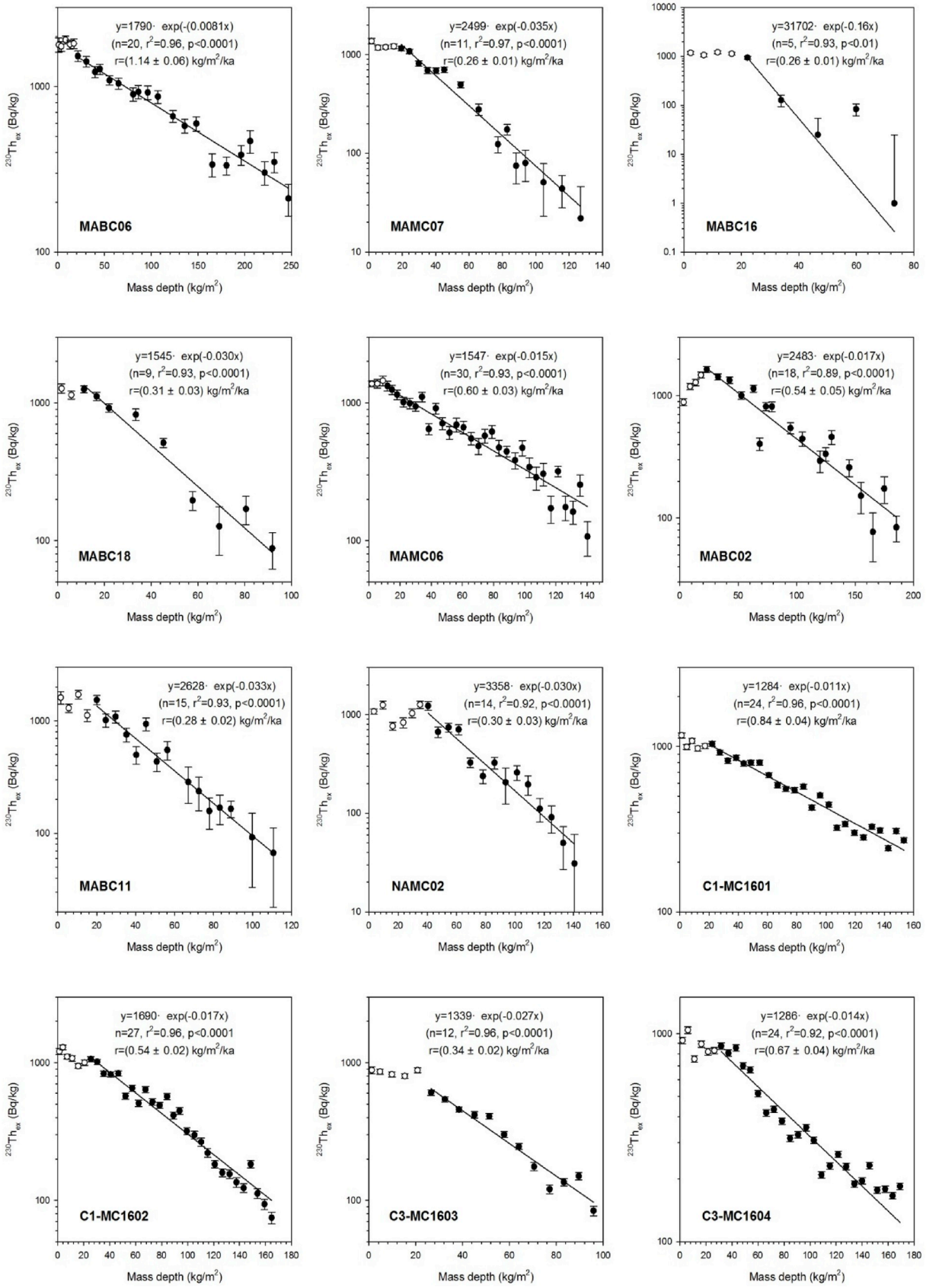

Fig. 5. The relationship between specific activity of $^{230}Th_{ex}$ (Bq/kg) and mass depth (kg/m^2) in sediment cores. The fitting curve and equation are shown. Note that data in the mixed layer are shown in open circles, which is excluded in calculation of sedimentation rate. The estimated mass accumulation rate are 1.14, 0.26, 0.26, 0.31, 0.60, 0.54, 0.28, 0.30, 0.84, 0.54, 0.34 and 0.67 kg/m^2/ka at stations MABC06, MAMC07, MABC16, MABC18, MAMC06, MABC02, MABC11, NAMC02, C1-MC1601, C1-MC1602, C3-MC1603 and C3-MC1604, respectively.

where the constant 10 represents conversion coefficient between both units.

The F_{orgC} values range from 0.10 to 4.52 g C/m^2/ka, with an average of 1.39 ± 1.19 g C/m^2/ka in our study areas (Table 1), which is slightly lower than those in the central equatorial Pacific (2.0–6.8 g C/m^2/ka, Müller and Suess, 1979) and the equatorial Pacific (1.8–18.8 g C/m^2/ka, Smith et al., 1997). Previous studies have shown that F_{orgC} correlated negatively with water depth on a global scale (Middelburg et al., 1997), but this correlation is not true around the seamounts of this study. However, a good positive correlation between F_{orgC} and s^* or r is observed, indicating that accumulation of organic matter was mainly controlled by sedimentation rate around the seamounts (Fig. 6).

3.3. Bioturbation coefficient derived from excess ^{210}Pb

3.3.1. Profiles of $^{210}Pb_{ex}$

The excess of ^{210}Pb ($^{210}Pb_{ex}$) represents the portion unsupported by ^{226}Ra in sediments, which is calculated as follows (Sanchez-Cabeza and Ruiz-Fernández, 2012):

$$^{210}Pb_{ex} = {}^{210}Pb - {}^{226}Ra \quad (13)$$

As shown in Fig. 7, specific activity of ^{210}Pb is excess with respect to its parent ^{226}Ra in the upper 30–50 cm at all stations, indicating the influence of bioturbation. Since the sedimentation rates are less than 2.50 mm/ka, ^{210}Pb will reach a radioactive equilibrium with ^{226}Ra within the upper several millimeters in absence of bioturbation. The prevalent excess of ^{210}Pb in the cores indicates that excess ^{210}Pb in newly deposits is transported to depth via bioturbation. At stations NAMC02, C1-MC1601, C1-MC1602 and C3-MC1604, the specific activity of $^{210}Pb_{ex}$ increases to a maximum as the depth increases, and then decreases exponentially (Fig. 7). The appearance of the maximum indicates a heterogeneous mixing of particles by the benthic organisms (Boudreau, 1986; Smith and Schafer, 1984; Yang and Zhou, 2004). The data of $^{210}Pb_{ex}$ affected by non-local mixing are excluded when estimating bioturbation coefficient.

3.3.2. Bioturbation coefficient

According to one-dimensional diffusion model, the bioturbation coefficient (D_B) is calculated by fitting $^{210}Pb_{ex}$ to the following function (Nozaki et al., 1977):

$$\frac{\partial}{\partial t}(\rho A) = \frac{\partial}{\partial t}\left(\rho D_B \frac{\partial A}{\partial z}\right) - \frac{\partial}{\partial z}(\rho s^* A) - \lambda \rho A \quad (14)$$

where ρ is density of sediments (g/cm^3), A is specific activity of $^{210}Pb_{ex}$, z is the depth below sediment-water interface (cm). D_B is bioturbation coefficient (cm^2/a), s^* is linear sedimentation rate (cm/a), λ is decay constant of ^{210}Pb (0.03118 a^{-1}).

Assuming: (1) a steady state, (2) D_B, s^* and ρ are constant in the mixed layer, and (3) s^* is low enough to be ignored during bioturbation, equation (14) is simplified as follows:

$$0 = D_B \frac{\partial^2 A}{\partial x^2} - \lambda A \quad (15)$$

By applying the boundary conditions, i.e., x → 0, A = A_0, and x → ∞, A → 0, the solution of equation (15) is:

$$A = A_0 e^{-z\sqrt{\frac{\lambda}{D_B}}} \quad (16)$$

The calculated D_B values range from 1.8-27.1 cm^2/a with an average of 10.8 ± 9.2 cm^2/a (Fig. 8). The bioturbation coefficients around the seamounts show highly variable on a small scale. For example, the D_B value at station MABC06 (27.1 ± 4.5 cm^2/a) is significantly larger than that at station MAMC07 (4.2 ± 0.7 cm^2/a) although the distance between two stations is only 2.3 km. Similarly, bioturbation in deep sea sediments also shows great spatial variability induced by benthos activities. For example, the D_B values showed changes in decimeter scale in the abyssal Arabian Sea (Turnewitsch et al., 2000), the Peru Basin (Suckow et al., 2001) and the northeast Atlantic (Smith et al., 1986), and varied 3–4 times at a site in the east equatorial Pacific (Cochran, 1985).

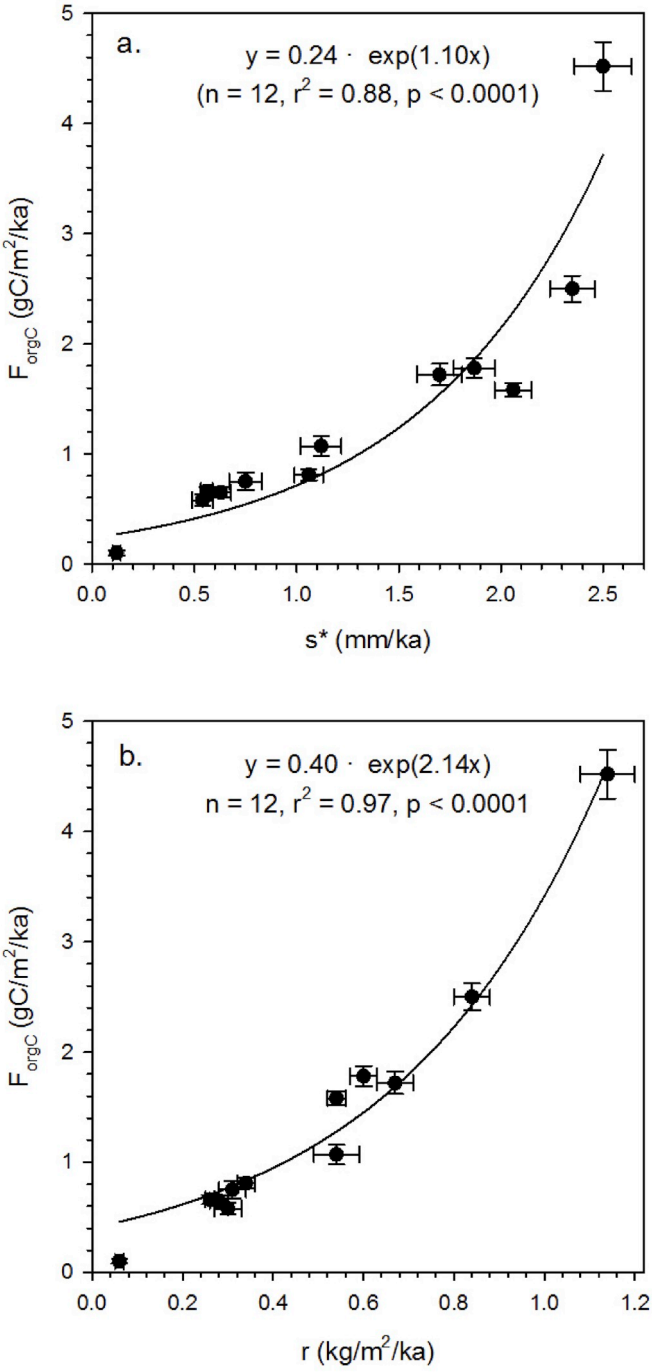

Fig. 6. The relationship between accumulation flux of organic carbon (gC/m^2/ka) and (a) linear sedimentation rate (mm/ka) and (b) mass accumulation rate (kg/m^2/ka) around the seamounts. The accumulation flux of organic carbon (F_{orgC}) shows an exponential increase with both linear sedimentation rate (s*) and mass accumulation rate (r). The fitting curve and equation are shown in each panel.

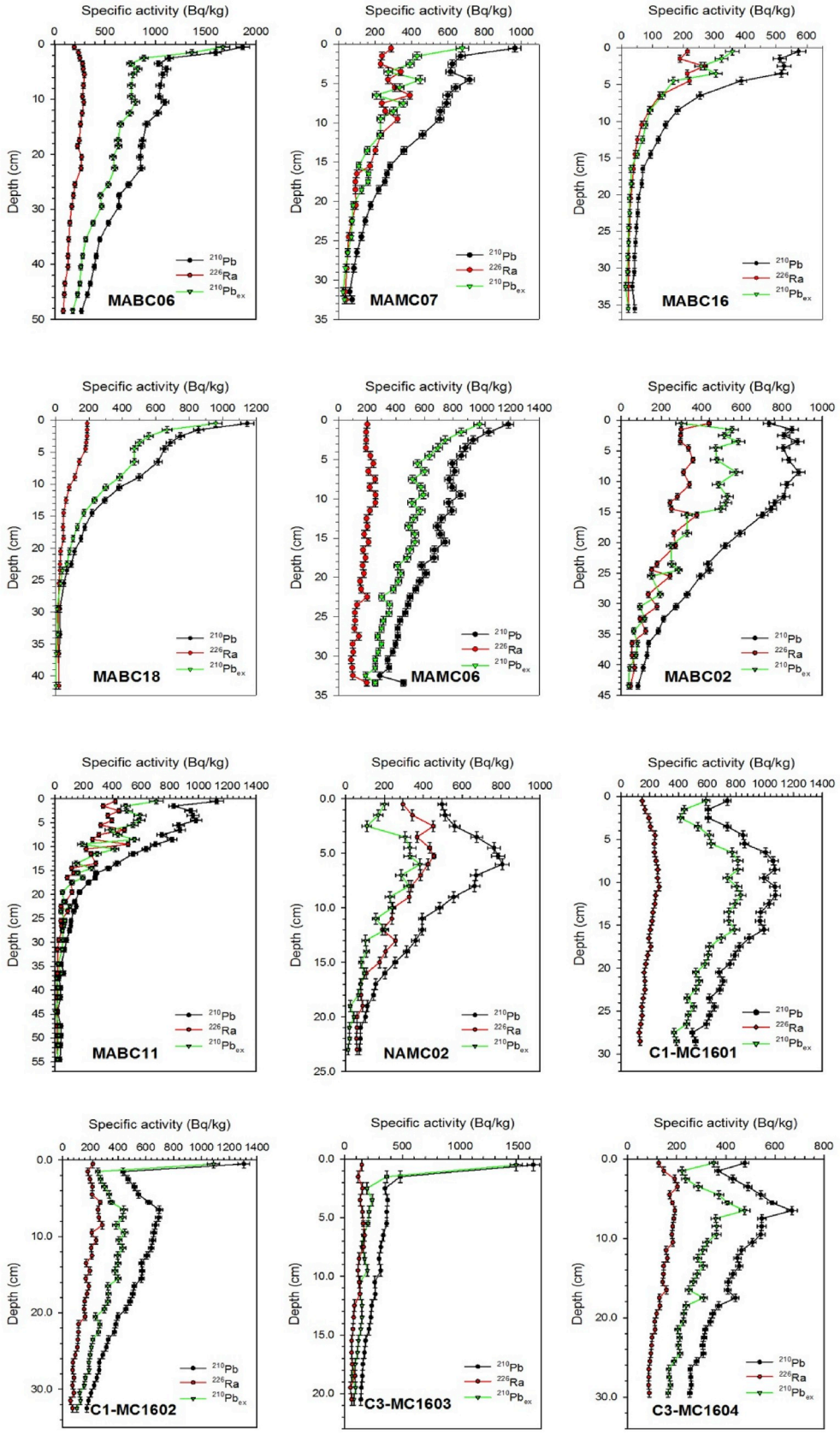

Fig. 7. Profiles of specific activity of ^{210}Pb, ^{226}Ra, ^{210}Pb$_{ex}$ (Bq/kg) in sediment cores. The specific activity of ^{210}Pb, ^{226}Ra and ^{210}Pb$_{ex}$ is represented by black circle, red diamond and green triangle, respectively. (For interpretation of the references to colour in this figure legend, the reader is referred to the Web version of this article.)

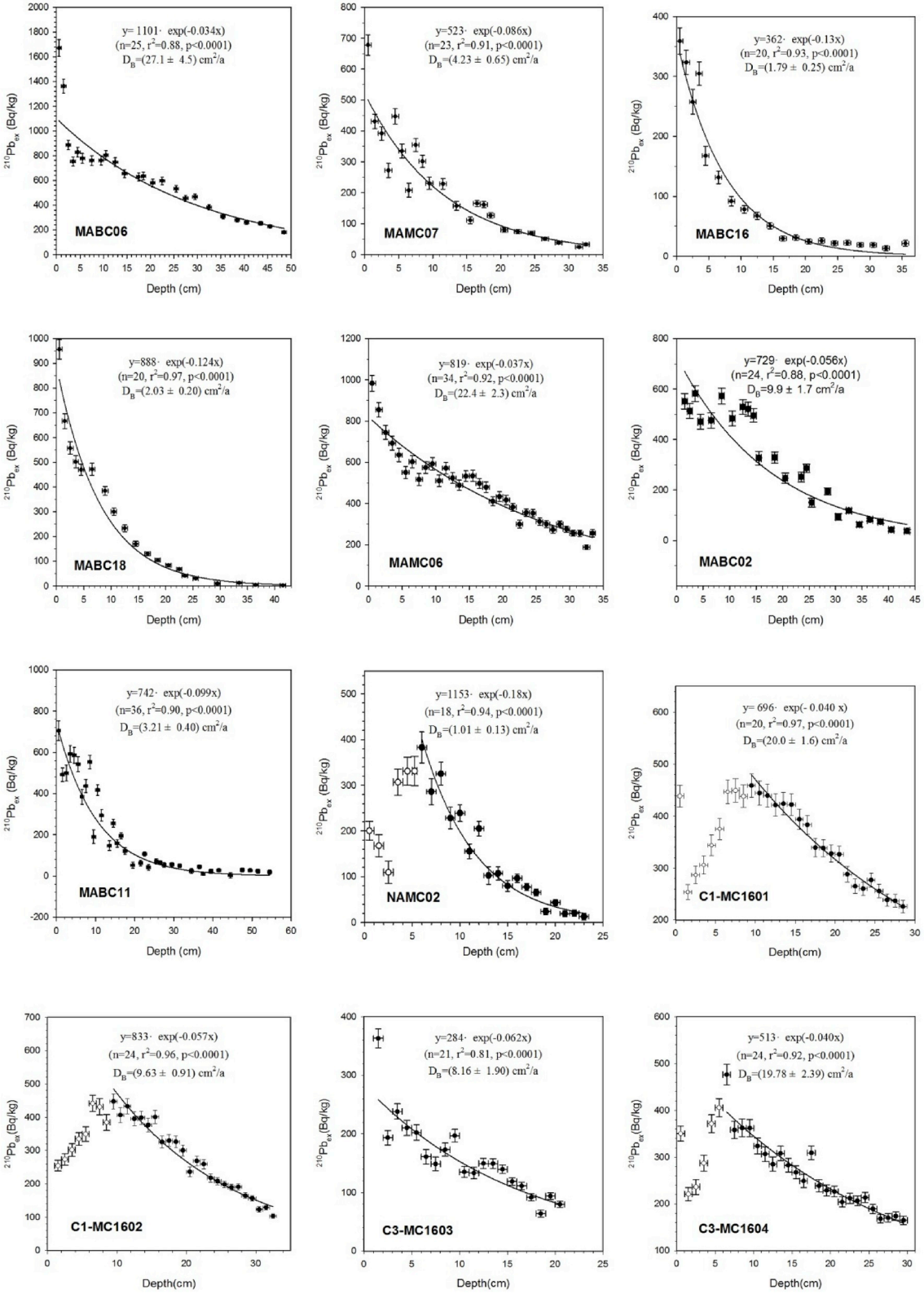

Fig. 8. The relationship between specific activity of $^{210}Pb_{ex}$ (Bq/kg) and depth (cm) in sediment cores. The fitting curve and equation are shown in each panel. Note that the data in the non-local mixing layer are shown in open circles, which is excluded in calculation of bioturbation coefficient. The estimated D_B values are 27.1, 4.23, 1.79, 2.03, 22.4, 9.9, 3.21, 1.01, 20.0, 9.63, 8.16 and 19.78 cm^2/a at stations MABC06, MAMC07, MABC16, MABC18, MAMC06, MABC02, MABC11, NAMC02, C1-MC1601, C1-MC1602, C3-MC1603 and C3-MC1604, respectively.

4. Discussion

4.1. Enhanced bioturbation around seamounts

As shown in Table 1, the D_B values around the seamounts in the northwest Pacific (1.8–27.1 cm^2/a, avg. 10.8 ± 9.2 cm^2/a) are higher than those in the western Pacific (1.59–8.64 cm^2/a, Yang et al., 2011), the northeast tropical Pacific (0.26–2.75 cm^2/a, Yang and Zhou, 2004), the equatorial Pacific (0.019–0.50 cm^2/a, Cochran, 1985; DeMaster and Cochran, 1982; Peng et al., 1979; Smith et al., 1997), the western North Pacific (0.11–0.58 cm^2/a, Yang et al., 1986), and the Santa Catalina Basin in the eastern North Pacific (0.33–0.59 cm^2/a, Smith et al., 1993), and close to those in productive areas, such as the Peru Basin (2.0–278.1 cm^2/a, Suckow et al., 2001), the Panama Basin (23 cm^2/a, Aller and DeMaster, 1984). The high D_B values indicate that bioturbation activity is active around seamounts, who are hotspots for pelagic organisms.

Previous studies have shown that as the water depth increases, the intensity of bioturbation is generally weakened, as most environmental factors affecting macrobenthos activity, such as particle size, sedimentation rate and food abundance, are often related to water depth. An empirical equation is proposed to describe the relationship between D_B and water depth (z, m) based on data from the eastern Pacific and the north Atlantic: $D_B = 5.2 \times 10^{0.762-0.0004\times z}$ (Middelburg et al., 1997). According to this equation, the D_B values around the seamounts in this study are estimated to be in a range of 0.13–0.45 cm^2/a, which is 1–2 orders of magntitude lower than those derived by excess ^{210}Pb. It means that biotubation around the seamounts is more active than those estimated by water depth.

The enhanced bioturbation is consistent with relatively high biomass of benthic organisms around seamounts. Several studies have shown that benthic abundance around seamounts is higher than that in the adjacent continental slopes and abyssal plains. For example, species richness around the seamounts of Norfolk ridge in the southwest Pacific is higher than that of adjacent Caledonia slope (Samadi et al., 2006). The megafaunal community around two seamounts of Andaman-arc basin in the northeast Indian Ocean is more diverse (Sautya et al., 2011), and the biomass of megabenthos around the seamount off Australia and New Zealand is higher than that in the adjacent slope (Rowden et al., 2010). The high benthic biomass indicates that seamounts are suitable for growth of benthic organisms.

Several environmental factors have been proposed to influence bioturbation in deep-sea sediments, including water depth (Middelburg et al., 1997), bottom current (Smith and Schafer, 1984), oxygen penetration into sediment (Smith and Rabouille, 2002), sedimentation rate (Boudreau, 1994; Tromp et al., 1995), organic carbon content in surface sediment (Yang and Zhou, 2004; Yang et al., 2011), and burial flux of particulate organic carbon at sediment-water interface (Legeleux et al., 1994; Pope et al., 1996; Smith et al., 1997; Smith and Rabouille, 2002). It is valuable to assess which factor regulates bioturbation in the unique environment of seamounts. Our results show a great positive correlation between the D_B value and the linear sedimentation rate (s^*) or mass accumulation rate (r) around the seamounts (Fig. 9 a, b), indicating sedimentation of particulate matter in the water column is a main process affecting the intensity of bioturbation. This positive correlation is similar to previous observation by compilation of global data (Boudreau, 1994; Tromp et al., 1995). However, the D_B values around the seamounts are significant higher than predicted from the empirical relationships based on global data (Fig. 9a). For example, the relationship between the D_B value and the linear sedimentation rate obtained in this study is $D_B = 1.1\times10^6 \cdot s^{1.3}$, whereas the reported empirical relationships are $D_B = 15.7 \cdot s^{0.6}$ (Boudreau, 1994) and $D_B = 42.66 \cdot s^{0.85}$ (Tromp et al., 1995). It is evident that the intensity of bioturbation around the seamounts is stronger than the empirical prediction. Note that the empirical relationships were based on data from different marine environments where only a little in low sedimentary environment, although the sedimentation rates varied by more than five orders of magnitude

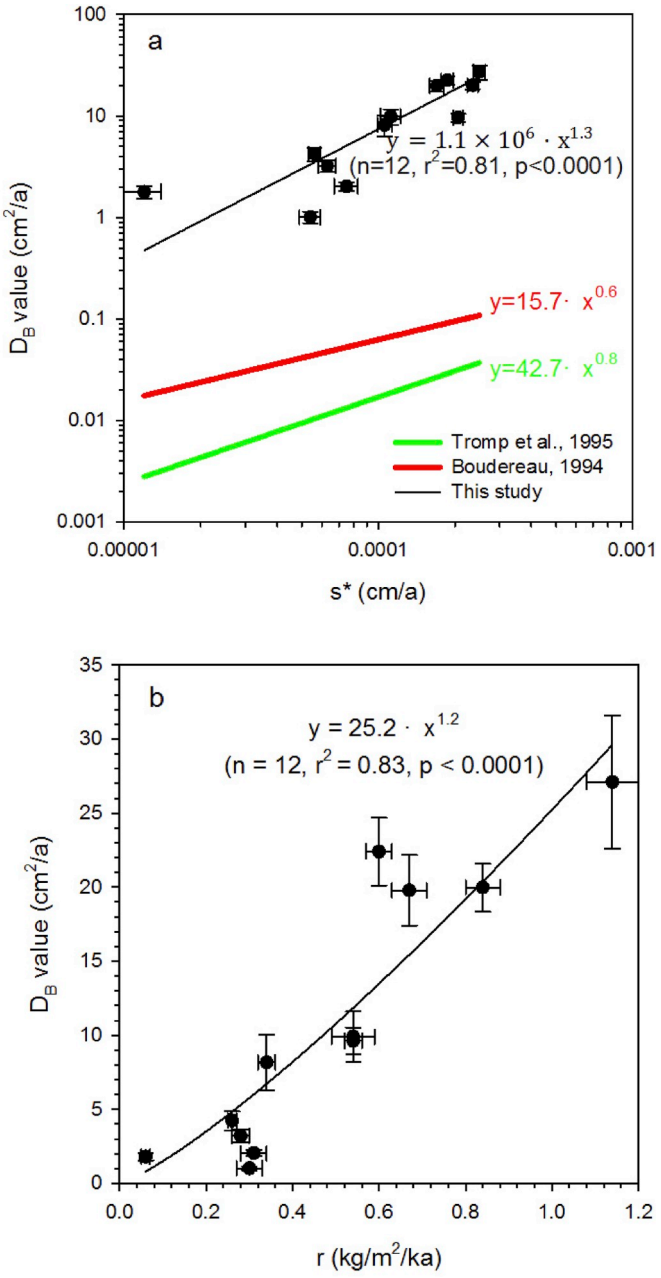

Fig. 9. The relationship between bioturbation coefficient (cm^2/a) and (a) linear sedimentation rate (mm/ka) and (b) mass accumulation rate ($kg/m^2/ka$) around the seamounts. The D_B values show an exponential increase with both the s^* and the r. In panel a, the black line is fitting curve of our data. The red and green lines represent the empirical equations proposed by Boudereau et al. (1994) and Tromp et al. (1995) respectively. (For interpretation of the references to colour in this figure legend, the reader is referred to the Web version of this article.)

(0.1–10^5 mm/ka, Boudreau, 1994; 1–10^5 mm/ka, Tromp et al., 1995). The sedimentation rates around the seamounts are in a range of 0.12–2.50 mm/ka, indicating that the enhanced bioturbation exists in the low sedimentary seamount environment.

The fact that bioturbation around the seamounts is regulated by sedimentation rate reflects the effect of changes in food supply required for the growth of benthic organisms. A good exponential positive relationship between the D_B values and accumulation fluxs of organic carbon was observed in this study, indicating that bioturbation around the seamounts was supported by accumulation of organic matter in

sediments (Fig. 10). Similar covariation relationship between bioturbation and accumulation flux of organic carbon have been observed in the equatorial Pacific, the western Pacific and the north Atlantic (Yang and Zhou, 2004; Yang et al., 2011). This means that similar to other sea areas, bioturbation around the seamounts is mainly affected by the availability of organic matter.

4.2. Spatial variation of bioturbation around the seamounts

As shown in Fig. 11, spatial distribution of the D_B around the seamounts shows that the highest value occurs at a certain distance from the edge of seamount summit, while the low values at the edge of summit and the abyssal plain far from the seamounts. The D_B values change by 26.8 times in a range of only 140 km from the seamount summit, indicating that bioturbation has high spatial variability around the seamounts. The highest value of D_B around the Pako Guyot appears about 40 km from the edge of seamount summit, while that around the Marcus-Wake seamounts appears about 50 km away from the edge of seamount summits (Fig. 11). As for the Pako Guyot, the depth of summit edge is 1650 m, and the uphill slope is 10.8° from 1650 m to 4000 m while the downhill slope is 2.8° from 4000 m to 5500 m. The estimated distance from the edge of summit to the foot of seamount is about 43 km for the Pako Guyot. Similarly, the distance from the edge of summits to the foot of seamounts is estiamted to be about 49 km for the Marcus-Wake seamounts (the depth of summit edge is 1300 m, and the uphill slope is 13° from 1300 m to 4200 m while the downhill slope is 2° from 4200 m to 5500 m). Obviously, all the highest D_B values appear at the foot of these seamounts.

We hypothesize that the higher D_B values occurred at the foot of seamounts are related to more active benthic activities caused by massive accumulation of organic matter. At the foot of seamounts, in addition to local deposits from the water column, organic matter in surface sediments is also supplemented by transportation down the slope. In the open ocean, organic matter in the seabed sediments mainly derives from photosynthesis of phytoplankton in the euphotic zone. The sinking flux of particulate organic carbon (POC) in the water column

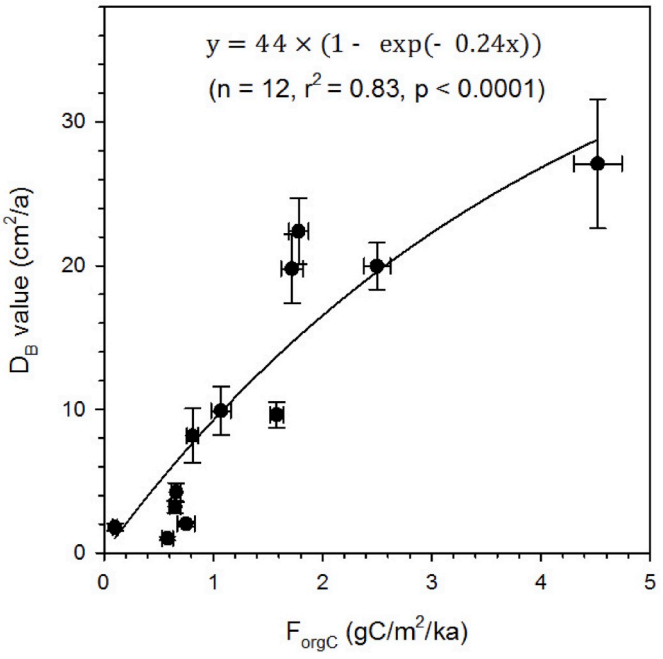

Fig. 10. The relationship between bioturbation coefficient (cm^2/a) and accumulation flux of organic carbon ($gC/m^2/ka$) around the seamounts. The D_B values show an exponential increase with the F_{orgC}. The fitting curve and equation are shown.

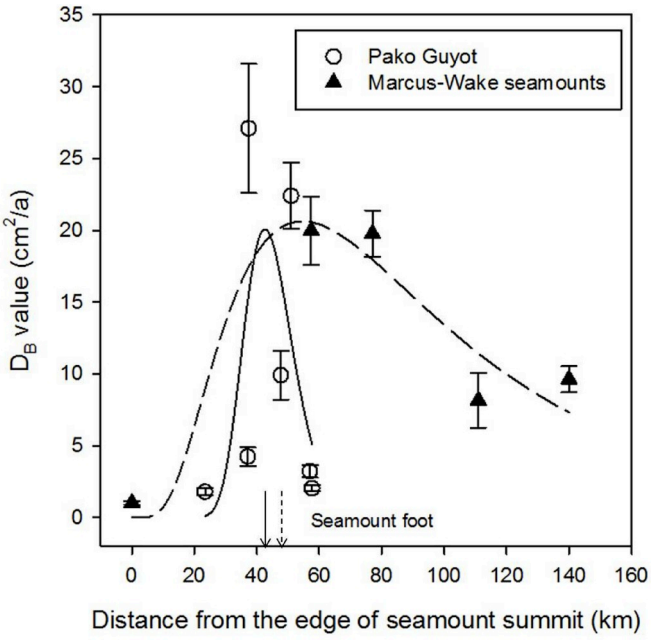

Fig. 11. The variation of bioturbation coefficient (cm^2/a) with the distance from the edge of the seamount summit (km). The open circles and solid triangles represent data from Pako Guyot and Marcus-Wake seamounts respectively. The solid and dashed lines are fitting curves for data from Pako Guyot and Marcus-Wake seamounts respectively. The solid and dashed arrows point to the foot of Pako Guyot and Marcus-Wake seamounts respectively.

decreases exponentially with increasing depth (Martin et al., 1987). According to a power-law model ($F_{POC}(z) = C \cdot z^{-b}$, Martin et al., 1987) and its ideal parameter value ($b \approx 0.7$, Cael and Bisson, 2018), the POC export fluxes at depths of 1600 m (the depth of Pako Guyot summit) and 1300 m (the depth of Marcus-Wake seamount summit) are estimated to be 2.4 and 2.7 times the flux at a depth of 5500 m (the depth of seamount foot), respectively. Clearly, the unique topographical feature of seamounts helps to capture more particulate organic matter on the summit and transport it down the hillside to form an organic-rich sedimentary environment at the foot of seamounts. The accumulation of organic matter stimulates benthic activity, thereby strengthening bioturbation at the foot of seamounts.

This variation pattern of the D_B values is consistent with the distribution of benthic organisms around the seamounts. In the voyage of Pako Guyot from July to September 2012, distribution of benthos around the seamount was investigated. The results showed that 63 species of megabenthos inhabit around the Pako Guyot, including 22 species of *Porifera* (sponges, etc.), 17 species of *Cnidaria* (corals, sea anemones, etc.), 15 species of *Echinodermata* (sea lily, starfish, brittle star, sea urchin, sea cucumber, etc.), *Arthropoda* (shrimp, etc.) and *Chordata* (fish, etc.). The density of macrobenthos decreases as the distance from the foot of Pako Guyot increases (Wang, 2015), which is similar to spatial variation of the D_B values observed here. This may indicate that macrobenthos are main groups affecting bioturbation in sediments around the Pako Guyot. Similarly, the D_B values have been observed to increase with the abundance of mega- and macro-benthos in the northeast tropical Atlantic (Legeleux et al., 1994) and the equatorial Pacific (Smith et al., 1997). The spatial distribution of benthic organisms is closely related to their lifestyle, current status, food supply, etc. The current observed by the mooring system indicated that the bottom velocity on the summit is higher than that at the foot of the Pako Guyot (Wang, 2015), which means that benthic organisms that cause bioturbation prefer a low-energy environment. Previous studies of benthic communities around seamounts have shown that filter feeding and sessile benthos (such as sponges and corals) prefer high-energy

environments (such as the summit or peak of seamounts) because rapid flow provides more rock outcrops for biofouling, while deposit feeders prefer soft sediments with weak currents, which facilitates particle settling (Clark et al., 2010; Kaufmann et al., 1989; McClain and Lundsten, 2015). Since the deposit feeder is the main biological population for bioturbation in sediments, the higher D_B values at the food of Pako Guyot is obviously related to the higher biomass of deposit feeders. As for the Marcus-Wake seamounts, due to the lack of benthic data, we can not discuss the impact of benthic organisms on the spatial variation of D_B values. Due to the limitation of benthic organisms, the possible effect of benthic habits and their bioturbation modes on bioturbation around the seamounts cannot be explored in this study. More simultaneous research on bioturbation and benthos is needed in the future.

5. Conclusions

Our results show an enhanced but highly variable bioturbation around the seamounts of the Magellan and Marcus-Wake clusters. The D_B values around the seamounts estimated by $^{210}Pb_{ex}$ tracer are higher than those in abyssal sediments or predicted by traditional empirical equations. The spatial variation shows that the highest D_B value occurs at about 40–50 km from the edge of the seamount summit, and the low D_B values at the edge of summit and the abyssal plain far from the seamounts. The active bioturbation at the foot of the seamounts is hypothesized to be related to massive accumulation of ogranic matter, which is supported by a positive relationship between the D_B value and the accumulation flux of organic carbon in surface sediments. The positive correlation between the D_B value and the linear sedimentation rate or mass accumulation rate further indicates that particle setting regulates organic matter accumulation around the seamounts. Climate change has changed oceanographic conditions and thus the flux of organic matter into the deep sea. More studies are needed to gain a deep understanding of bioturbation in seamounts in the context of future climate change.

Declaration of competing interest

The authors declare that they have no known competing financial interests or personal relationships that could have appeared to influence the work reported in this paper.

Acknowledgements

We sincerely appreciate China Ocean Mineral Resources R&D Association for organizing the field work and the crew of the RV *HAIYANG LIUHAO* and *DONGFANGHONG SHIHAO* for their assistance in sample collection. This work was supported by a Chinese COMRA program (No. DY135-13-E2-03) and the National Natural Science Foundation of China (No. 41721005).

References

Aller, R.C., DeMaster, D.J., 1984. Estimates of particle flux and reworking at the deep-sea floor using $^{234}Th/^{238}U$ disequilibrium. Earth Planet. Sci. Lett. 67 (3), 308–318.
Arndt, S., Jorgensen, B.B., LaRowe, D.E., Middelburg, J.J., Pancost, R.D., Regnier, P., 2013. Quantifying the degradation of organic matter in marine sediments: a review and synthesis. Earth Sci. Rev. 123, 53–86.
Berger, W.H., Adelseck, C.G., Mayer, L.A., 1976. Distribution of carbonate in surface sediments of the Pacific Ocean. J. Geophys. Res. 81 (15), 2617–2627.
Boudreau, B.P., 1994. Is burial velocity a master parameter for bioturbation? Geochem. Cosmochim. Acta 58 (4), 1243–1249.
Boudreau, B.P., 1998. Mean mixed depth of sediments: the wherefore and the why. Limnol. Oceanogr. 43 (3), 524–526.
Boudreau, B.P., Choi, J., Meysman, F., Frederique, C., 2001. Diffusion in a lattice-automaton model of bioturbation by small deposit feeders. J. Mar. Res. 59 (5), 749–768.
Boudreau, B.P., 1986. Mathematics of tracer mixing in sediments: I. Spatially-dependent, diffusive mixing. Am. J. Sci. 286 (3), 161–198.
Cael, B.B., Bisson, K., 2018. Particle flux parameterizations: quantitative and mechanistic similarities and differences. Front. Mar. Sci. 5, 395. https://doi.org/10.3389/fmars.2018.00395.
Chakrabarty, D., Das, S.K., 2007. Bioturbation-induced phosphorous release from an insoluble phosphate source. Biosystems 90 (2), 309–313.
Charbit, S., Rabouille, C., Siani, G., 2002. Effects of benthic transport processes on abrupt climatic changes recorded in deep-sea sediments: a time-dependent modeling approach. J. Geophys. Res. Oceans 107 (C11), 3194. https://doi.org/10.1029/2000JC000575.
Chen, M., Huang, Y.P., Cai, P.H., Guo, L.D., 2003. Particulate organic carbon export fluxes in the Canada Basin and Bering Sea as derived from $^{234}Th/^{238}U$ disequilibria. Arctic 56 (1), 32–44.
Clark, M.R., Rowden, A.A., Schlacher, T., Williams, A., Consalvey, M., Stocks, K.I., Rogers, A.D., O'Hara, T.D., White, M., Shank, T.M., Hall-Spencer, J.M., 2010. The ecology of seamounts: structure, function, and human impacts. Ann. Rev. Mar. Sci. 2 (2), 253–278.
Cochran, J.K., 1985. Particle mixing rates in sediments of the eastern equatorial Pacific: evidence from ^{210}Pb, $^{239, 240}Pu$ and ^{137}Cs distributions at MANOP sites. Geochem. Cosmochim. Acta 49 (5), 1195–1210.
DeMaster, D.J., Cochran, J.K., 1982. Particle mixing rates in deep-sea sediments determined from excess ^{210}Pb and ^{32}Si profiles. Earth Planet. Sci. Lett. 61 (2), 257–271.
Druffel, E.R.M., Williams, P.M., Livingston, H.D., Koide, M., 1984. Variability of natural and bomb-produced radionuclide distributions in abyssal red clay sediments. Earth Planet. Sci. Lett. 71 (2), 205–214.
Gilmore, G., 2008. Practical Gamma-Ray Spectroscopy. John Wiley & Sons.
Guinasso, N., Schink, D., 1975. Quantitative estimates of biological mixing rates in abyssal sediments. J. Geophys. Res. 80 (21), 3032–3043.
Henderson, G.M., Lindsay, F.N., Slowey, N.C., 1999. Variation in bioturbation with water depth on marine slopes: a study on the Little Bahamas Bank. Mar. Geol. 160 (1), 105–118.
Hutson, W.H., 1980. Bioturbation of deep-sea sediments: oxygen isotopes and stratigraphic uncertainty. Geology 8 (3), 127–130.
Kaufmann, R.S., Wakefield, W.W., Genin, A., 1989. Distribution of epibenthic megafauna and lebensspuren on two central North Pacific seamounts. Deep-Sea Res. Part I Oceanogr. Res. Pap. 36 (12), 1863–1896.
Kristensen, E., Penha-Lopes, G., Delefosse, M., Valdemarsen, T., Quintana, C.O., Banta, G. T., 2012. What is bioturbation? The need for a precise definition for fauna in aquatic sciences. Mar. Ecol. Prog. Ser. 446, 285–302.
Lecroart, P., Maire, O., Schmidt, S., Grémare, A., Anschutz, P., Meysman, F.J., 2010. Bioturbation, short-lived radioisotopes, and the tracer-dependence of biodiffusion coefficients. Geochem. Cosmochim. Acta 74 (21), 6049–6063.
Legeleux, F., Reyss, J.-L., Schmidt, S., 1994. Particle mixing rates in sediments of the northeast tropical Atlantic: evidence from $^{210}Pb_{xs}$, ^{137}Cs, $^{228}Th_{xs}$ and $^{234}Th_{xs}$ downcore distributions. Earth Planet. Sci. Lett. 128 (3), 545–562.
Leuschner, D.C., Sirocko, F., Grootes, P.M., Erlenkeuser, H., 2002. Possible influence of zoophycos bioturbation on radiocarbon dating and environmental interpretation. Mar. Micropaleontol. 46 (1–2), 111–126.
Levin, L.A., Thomas, C.L., 1989. The influence of hydrodynamic regime on infaunal assemblages inhabiting carbonate sediments on central Pacific seamounts. Deep Sea Research Part I. Oceanogr. Res. Pap. 36 (12), 1897–1915.
Lohrer, A.M., Thrush, S.F., Gibbs, M.M., 2004. Bioturbators enhance ecosystem function through complex biogeochemical interactions. Nature 431 (7012), 1092–1095.
Martin, J.H., Knauer, G.A., Karl, D.M., Broenkow, W.W., 1987. VERTEX: carbon cycling in the northeast Pacific. Deep Sea Res. A. 34, 267–285.
Matsumoto, E., Wong, C., 1977. Heavy metal sedimentation in Saanich Inlet measured with ^{210}Pb technique. J. Geophys. Res. 82 (34), 5477–5482.
McClain, C.R., 2010. Seamounts: identity crisis or split personality? J. Biogeogr. 34 (12), 2001–2008.
McClain, C.R., Lundsten, L., 2015. Assemblage structure is related to slope and depth on a deep offshore Pacific seamount chain. Mar. Ecol. 36 (2), 210–220.
Meadows, P.S., Meadows, A., Murray, J.M.H., 2012. Biological modifiers of marine benthic seascapes: their role as ecosystem engineers. Geomorphology 157–158, 31–48.
Meysman, F.J., Boudreau, B.P., Middelburg, J.J., 2003. Relations between local, nonlocal, discrete and continuous models of bioturbation. J. Mar. Res. 61 (3), 391–410.
Middelburg, J.J., Soetaert, K., Herman, P.M.J., 1997. Empirical relationships for use in global diagenetic models. Deep Sea Res. Oceanogr. Res. Pap. 44 (2), 327–344.
Müller, P.J., Suess, E., 1979. Productivity, sedimentation rate, and sedimentary organic matter in the oceans I. Organic carbon preservation. Deep Sea Res. Oceanogr. Res. Pap. 26 (12), 1347–1362.
Nozaki, Y., Cochran, K.J., Turekian, K.K., Keller, G., 1977. Radiocarbon and ^{210}Pb distribution in submersible-taken deep-sea cores from Project FAMOUS. Earth Planet. Sci. Lett. 34 (2), 167–173.
Peng, T.H., Broecker, W.S., Berger, W.H., 1979. Rates of benthic mixing in deep-sea sediment as determined by radioactive tracers. Quat. Res. 11 (1), 141–149.
Pope, R., DeMaster, D., Smith, C., Seltmann Jr., H., 1996. Rapid bioturbation in equatorial Pacific sediments: evidence from excess ^{234}Th measurements. Deep Sea Res. Part II Top. Stud. Oceanogr. 43 (4), 1339–1364.
Rea, D.K., 1994. The paleoclimatic record provided by eolian deposition in the deep sea: the geologic history of wind. Rev. Geophys. 32 (2), 159–195.
Reed, D.C., Huang, K., Boudreau, B.P., Meysman, F.J.R., 2006. Steady-state tracer dynamics in a lattice-automaton model of bioturbation. Geochem. Cosmochim. Acta 70 (23), 5855–5867.

Rowden, A.A., Schlacher, T.A., Williams, A., Clark, M.R., Stewart, R., Althaus, F., Bowden, D.A., Consalvey, M., Robinson, W., Dowdney, J., 2010. A test of the seamount oasis hypothesis: seamounts support higher epibenthic megafaunal biomass than adjacent slopes. Mar. Ecol. 31, 95–106.

Sanchez-Cabeza, J.A., Ruiz-Fernández, A.C., 2012. ^{210}Pb sediment radiochronology: an integrated formulation and classification of dating models. Geochem. Cosmochim. Acta 82, 183–200.

Samadi, S., Bottan, L., Macpherson, E., De Forges, B.R., Boisselier, M.C., 2006. Seamount endemism questioned by the geographic distribution and population genetic structure of marine invertebrates. Mar. Biol. 149 (6), 1463–1475.

Sautya, S., Ingole, B., Ray, D., Stöhr, S., Samudrala, K., Raju, K.K., Mudholkar, A., 2011. Megafaunal community structure of Andaman seamounts including the Back-arc Basin – a quantitative exploration from the Indian Ocean. PLoS One 6 (1), e16162.

Shull, D.H., 2001. Transition-matrix model of bioturbation and radionuclide diagenesis. Limnol. Oceanogr. 46 (4), 905–916.

Smith, C.R., Berelson, W., Demaster, D.J., Dobbs, F.C., Hammond, D., Hoover, D.J., Pope, R.H., Stephens, M., 1997. Latitudinal variations in benthic processes in the abyssal equatorial Pacific: control by biogenic particle flux. Deep Sea Res. Part II Top. Stud. Oceanogr. 44 (9–10), 2295–2317.

Smith, C.R., Hoover, D.J., Doan, S.E., Pope, R.H., Demaster, D.J., Dobbs, F.C., Altabet, M. A., 1996. Phytodetritus at the abyssal seafloor across 10° of latitude in the central equatorial Pacific. Deep Sea Res. Part II Top. Stud. Oceanogr. 43 (4–6), 1309–1338.

Smith, C.R., Pope, R.H., DeMaster, D.J., Magaard, L., 1993. Age-dependent mixing of deep-sea sediments. Geochem. Cosmochim. Acta 57 (7), 1473–1488.

Smith, C.R., Rabouille, C., 2002. What controls the mixed-layer depth in deep-sea sediments? The importance of POC flux. Limnol. Oceanogr. 47 (2), 418–426.

Smith, J.N., Boudreau, B.P., Noshkin, V., 1986. Plutonium and ^{210}Pb distributions in northeast Atlantic sediments: subsurface anomalies caused by non-local mixing. Earth Planet. Sci. Lett. 81 (1), 15–28.

Smith, J.N., Schafer, C., 1984. Bioturbation processes in continental slope and rise sediments delineated by ^{210}Pb, microfossil and textural indicators. J. Mar. Res. 42 (4), 1117–1145.

Smoot, N.C., 1989. The Marcus-Wake seamounts and guyots as paleofracture indicators and their relation to the Dutton Ridge. Mar. Geol. 88 (1), 117–131.

Suckow, A., Treppke, U., Wiedicke, M.H., Weber, M.E., 2001. Bioturbation coefficients of deep-sea sediments from the Peru Basin determined by gamma spectrometry of $^{210}Pb_{exc}$. Deep Sea Res. Part II Top. Stud. Oceanogr. 48 (17), 3569–3592.

Teal, L.R., Bulling, M.T., Parker, E.R., Solan, M., 2008. Global patterns of bioturbation intensity and mixed depth of marine soft sediments. Aquat. Biol. 2 (3), 207–218.

Tromp, T.K., Van Cappellen, P., Key, R.M., 1995. A global model for the early diagenesis of organic carbon and organic phosphorus in marine sediments. Geochem. Cosmochim. Acta 59 (7), 1259–1284.

Turnewitsch, R., Falahat, S., Nycander, J., Dale, A., Scott, R.B., Furnival, D., 2013. Deep-sea fluid and sediment dynamics - influence of hill- to seamount-scale seafloor topography. Earth Sci. Rev. 127, 203–241.

Turnewitsch, R., Witte, U., Graf, G., 2000. Bioturbation in the abyssal Arabian Sea: influence of fauna and food supply. Deep-Sea Res. Part II Top. Stud. Oceanogr. 47 (14), 2877–2911.

Wang, C., 2015. Research Report on the Environmental Gradient of the Cobalt-Rich Crust Exploration Areas and its Influence on the Benthic Zonal Distribution. China Ocean Mineral Resources R&D Association (in chinese).

Wang, Y., Zhang, H., Liu, J., Zhang, X., Zhu, B., 2016. Abundances and spatial distributions of associated useful elements in co-rich crusts from caiwei seamount in magellan seamounts. Mar. Geol. Quat. Geol. 36 (2), 65–74 (in chinese).

Wessel, P., Sandwell, D.T., Kim, S.-S., 2010. The global seamount census. Oceanography 23 (1), 24–33.

Wheatcroft, R., Jumars, P., Smith, C., Nowell, A., 1990. A mechanistic view of the particulate biodiffusion coefficient: step lengths, rest periods and transport directions. J. Mar. Res. 48 (1), 177–207.

Wheatcroft, R.A., 1992. Experimental tests for particle size-dependent bioturbation in the deep ocean. Limnol. Oceanogr. 37 (1), 90–104.

Williams, P.M., Stenhouse, M.C., Druffel, E.M., Koide, M., 1978. Organic ^{14}C activity in an abyssal marine sediment. Nature 276 (5689), 698–701.

Wilson Jr., R.R., Kaufmann, R.S., Atolls, 1987. Seamount biota and biogeography. Seamounts Islands & Atolls 43, 355–377.

Windom, H.L., 1975. Eolian contributions to marine sediments. J. Sediment. Res. 45 (2), 520–529.

Yang, H.-S., Nozaki, Y., Sakai, H., Nagaya, Y., Nakamura, K., 1986. Natural and man-made radionuclide distributions in Northwest Pacific deep-sea sediments: rates of sedimentation, bioturbation and ^{226}Ra migration. Geochem. J. 20 (1), 29–40.

Yang, Q., Zhou, H., 2004. Bioturbation in near-surface sediments from the COMRA Polymetallic Nodule Area: evidence from excess ^{210}Pb measurements. Chin. Sci. Bull. 49 (23), 2538–2542.

Yang, W.F., Zhang, X.X., Chen, M., Wang, Z., Wang, C.S., Huang, Y.P., Zhang, D.S., Qiu, Y.S., 2011. Bioturbation in the western Pacific Ocean: use of ^{210}Pb to evaluate intensity and POC transport. J. Cent. South Univ. 42 (Suppl. 2), 189–195 (in chinese).

Yang, W., Chen, M., Zhang, X.X., Guo, Z.G., Li, G.X., Ma, Q., Yang, J.H., Huang, Y.P., 2013. Thorium isotopes (^{228}Th, ^{230}Th, ^{232}Th) and applications in reconstructing the Yangtze and Yellow River floods. Int. J. Sediment Res. 28 (4), 588–595.

Yesson, C., Clark, M.R., Taylor, M.L., Rogers, A.D., 2011. The global distribution of seamounts based on 30 arc seconds bathymetry data. Deep Sea Res. Oceanogr. Res. Pap. 58 (4), 442–453.

Zhang, L., Chen, M., Yang, W.F., Xing, N., Li, Y.P., Qiu, Y.S., Huang, Y.P., 2004. Size-fractionated thorium isotopes (^{228}Th, ^{230}Th, ^{232}Th) in surface waters in the Jiulong River estuary, China. J. Environ. Radioact. 78 (2), 199–216.

Zhu, B.D., Liang, D.H., Cui, Z.G., 2011. Geomorphologic characteristics and genesis of Magellan seamount chain in the western Pacific. J. Cent. South Univ. 42 (Suppl. 2), 92–98 (in chinese).